

Dual-Chirality Helical Nanobelts: Linear-to-Rotary Motion Converters for Three-Dimensional Microscopy

Lixin Dong, *Member, IEEE*, Li Zhang, Bradley E. Kratochvil, *Student Member, IEEE*, Kaiyu Shou, and Bradley J. Nelson, *Senior Member, IEEE*

Abstract—A linear-to-rotary motion converter is demonstrated using 3-D SiGe/Si dual-chirality helical nanobelts (DCHNBs). Analytical and experimental investigation shows that the motion conversion has excellent linearity for small deflections. The conversion ratios of displacement and load for a SiGe/Si DCHNB (an 8-nm-thick Si_{0.6}Ge_{0.4} and a 10-nm-thick Si layer) are found to be 171.3°/μm and 2.110 × 10⁻⁶ N · m/N, respectively. The stiffness (0.033 N/m) is much smaller than that of bottom-up synthesized helical nanostructures, which is promising for high-resolution force measurement in nanoelectromechanical systems. To perform torque measurement, two atomic force microscope cantilevers are used for simultaneous characterization of axial and radial properties of the same nanostructure. An application related to 3-D imaging is shown in a scanning electron microscope. The ultracompact size makes it possible for DCHNBs to serve as rotary stages for creating 3-D scanning probe microscopes or microgoniometers. [2009-0045]

Index Terms—Helical nanobelt (HNB), microgoniometer, motion converter, nanoelectromechanical systems (NEMS), 3-D scanning probe microscope (SPM).

I. INTRODUCTION

MECHANICAL motion, particularly resonance, is at the core of many nanoelectromechanical systems (NEMS) [1]–[6] that are envisioned, and conversion between various forms of motions will play an important role in future nanosystem applications. Motion converters have been widely used for millennia to transmit actuator motion at different speeds and torques or in different directions. Typical examples include such pairs as pinion–gear, pinion–rack, pinion–worm, wheel–belt, wheel–chain, cable–pulley, and linkage mechanisms. The most commonly used mechanisms for converting linear motion to rotary motion use a piston moving in a cylinder

Manuscript received February 16, 2009; revised May 22, 2009. First published September 16, 2009; current version published September 30, 2009. This work was supported by the Swiss Federal Institute of Technology (ETH) Zurich. Subject Editor A. J. Ricco.

L. Dong was with the Institute of Robotics and Intelligent Systems, Swiss Federal Institute of Technology (ETH) Zurich, 8092 Zurich, Switzerland. He is currently with the Department of Electrical and Computer Engineering, Michigan State University, East Lansing, MI 48824-1226 USA (e-mail: ldong@msu.edu).

L. Zhang, B. E. Kratochvil, K. Shou, and B. J. Nelson are with the Institute of Robotics and Intelligent Systems, Swiss Federal Institute of Technology (ETH) Zurich, 8092 Zurich, Switzerland (e-mail: bnelson@ethz.ch).

Color versions of one or more of the figures in this paper are available online at <http://ieeexplore.ieee.org>.

Digital Object Identifier 10.1109/JMEMS.2009.2029975

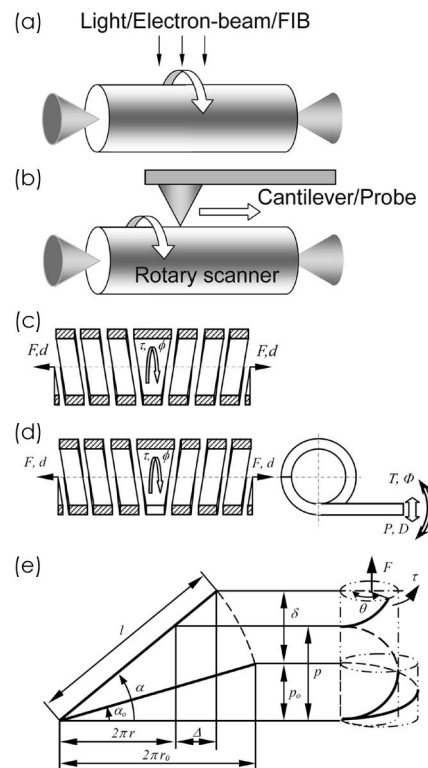


Fig. 1. Motion converters using DCHNBs. (a) Linear-to-rotary motion converter for 3-D microscopy using an irradiation source (light, electron beam, or FIB). (b) Linear-to-rotary motion converter for 3-D SPM. (c) Linear-to-rotary motion converter using a DCHNB. (d) Transmission converting linear motion to extended linear (small displacement)/rotary (large displacement) motion. (e) One-pitch helix under an axial extension force. Three-dimensional and plan view show how the geometry changes from the initial position (radius r_0 , pitch angle α_0) to the deflected position (radius r , pitch angle α) with a deflection δ and an induced rotational angle θ .

to rotate a crank shaft by means of a link. It is interesting to note that at molecular scales in nature, similar converters also play an important role in motion conversion [7].

One application area of motion conversion is for 3-D microscopy, in which samples are rotated [Fig. 1(a)] so that different views are exposed to light, electron beams, or focused-ion beams (FIBs). Conventional rotary/tilt stages usually consist of gear trains, bearings, and other elements actuated by motors. Due to the clearance of the motion pairs and the deviation between the optical and rotary axes, it is commonly required to readjust the imaging field, focal plane, and other parameters.

Furthermore, due to mechanical constraints, a 360° rotation is extremely difficult to achieve, leaving some aspects inaccessible. Goniometry has been an important technique in transmission electron microscopes (TEMs) for obtaining electron diffraction patterns, high-resolution images, and tomography, but conventional goniometers do not generate more than 60° rotations. Tilt stages of scanning electron microscopes (SEMs) and tilt holders of TEMs suffer with similar limits.

Nanoscale rotary motion can also be applied to other forms of microscopy. Scanning tunneling microscopy (STM) [8], atomic force microscopes (AFMs) [9], and other scanning probe microscopes (SPMs) allow us to perform tasks such as characterization [10], manipulation [11], and fabrication [12], [13], in addition to imaging, on single molecules, atoms, and bonds, thereby providing a tool that operates at the ultimate limits of manufacturing. While tremendous progress [14], [15] has been made in enhancing their spatial resolution, sensing mechanisms, and probe tips [16]–[18], less attention has been paid to their conventional X-Y planar scanning stages [19], which are best suited for features on a planar surface. Investigation of freestanding individual nanostructures is becoming increasingly important due to the possibility of avoiding a side effect from the substrate on the specimen. A single-walled carbon nanotube freely suspended over a trench has been investigated with atomic resolution using an STM [20] and correlated to electrical transport measurement [21]. A rotary scanning stage will enable the exposure of different aspects of an individual nanostructure to the probe tip, essentially creating a 3-D SPM [Fig. 1(b)], for fully correlating atomic structures and physical properties.

Due to the difficulty in generating precise rotation without clearance issues or backlash, linear-to-rotary motion converters would be an effective way to realize rotation from a linear actuator, which is generally easier to achieve at nanometer resolutions using solid-state actuators such as piezoelectrics. Among various nano building blocks, 3-D helical nanostructures, such as helical carbon nanotubes [22], coiled ZnO nanobelts [23], and rolled-up semiconductive nanostructures [24]–[28], have attracted intense research interest because of their special morphology and electromechanical properties for potential applications in NEMS [28], [29] and nanoelectronic devices [30] as springs, electromagnets, inductors, resonators, sensors, and actuators. Here, we demonstrate one type of these helical nanostructures, dual-chirality helical nanobelts (DCHNBs), as a transmission for converting between linear and rotary motion.

II. DESIGN OF MOTION CONVERTERS

As schematically shown in Fig. 1(c), the motion converter consists of a DCHNB with a left-handed and a right-handed part. By linearly extending the two ends of the DCHNB, the central part outputs rotary motion; providing a unique and fundamental mechanical mechanism for realizing linear-to-rotary motion conversion, a property not previously demonstrated in other nanostructures. With an extended arm [Fig. 1(d)], the output can be linear (small displacement) or rotary (large displacement) motion.

As shown in Fig. 1(d), we define the ratio between the output torque τ and input force F as the load conversion ratio, i.e., $R_F = \tau/F$, and between the output angular displacement ϕ and the input extension d as the displacement conversion ratio, i.e., $R_d = \phi/d$. The extended arm [Fig. 1(e)] amplifies the output further into linear (small displacement) motion with a force P and displacement D , or rotary (large displacement) motion with a torque T and a rotation Φ . We define r_0 , p_0 , and α_0 as the radius, pitch, and pitch angle, respectively, of the initial DCHNB. When a tensile force F is applied to the DCHNB, it elongates and rotates about the unwinding direction. At this deflected state, r , p , and α indicate the radius, pitch, and pitch angle, respectively. According to the plan view of a one-pitch DCHNB as shown in Fig. 1(e), the unwinding angle ϕ of a DCHNB is given by [31]

$$\phi = n\theta = 2\pi n \left(\frac{r_0 \cos \alpha}{r \cos \alpha_0} - 1 \right) \quad (1)$$

where n is the number of turns of a half-DCHNB [right-handed part in Fig. 1(e)]. Considering the mirror symmetry, the other half with opposite chirality has the same unwinding angle.

Once the DCHNB is elongated $2d$, each half of the DCHNB will deflect d . For each turn, the deflection will be $\delta = d/n$. According to the geometry, if one assumes that the length of the nanobelt L of a half-DCHNB (the length per turn: $l = L/n$) is constant (which is reasonable for springs with a large index [31]), the number of turns of the deformed DCHNB m will be

$$m = \frac{r}{r_0} \sqrt{1 - \frac{d}{n\pi r_0} \tan \alpha_0 - \frac{d^2}{4n^2\pi^2 r_0^2}} n. \quad (2)$$

Noting that $\phi = 2\pi(m - n)$ and $p_0 = 2\pi r_0 \tan \alpha_0$, the unwinding angle ϕ can be expressed as a function of d

$$\phi = 2\pi n \left(\frac{r}{r_0} \sqrt{1 - \left(2 + \frac{d}{np_0}\right) \frac{d}{np_0} \tan^2 \alpha_0} - 1 \right) \quad (3)$$

with a geometric constraint of

$$\left(-1 - \sqrt{1 + \cot^2 \alpha_0}\right) np_0 \leq d \leq \left(-1 + \sqrt{1 + \cot^2 \alpha_0}\right) np_0. \quad (4)$$

For small deflection, the change of the radius of a DCHNB can be ignored [$\Delta \approx 0$ in Fig. 1(e)], i.e., $r \approx r_0$.

As an example, for a DCHNB with $\alpha_0 = 58^\circ$, $p_0 = 5.4 \mu\text{m}$, and $n = 7$, we can depict ϕ versus d [Fig. 2(a)]. It can be seen that the linear range is quite large before the DCHNB straightens (see the inset of Fig. 2(a) for long range ϕ versus d curve). An accurate displacement conversion ratio can be obtained from (3): $R_d = \phi/d = 179.4^\circ/\mu\text{m}$ or 3.75 turn/pitch.

III. DISPLACEMENT CONVERSION

The fabrication process for helical nanobelts (HNBs) by the scrolling of strained SiGe/Si or InGaAs/GaAs bilayer has been reported elsewhere [27], [28]. Based on V-shaped mesa designs [inset of Fig. 2(b)], freestanding DCHNBs can be achieved [25]. Fig. 3(a) shows an as-fabricated SiGe/Si DCHNB with a

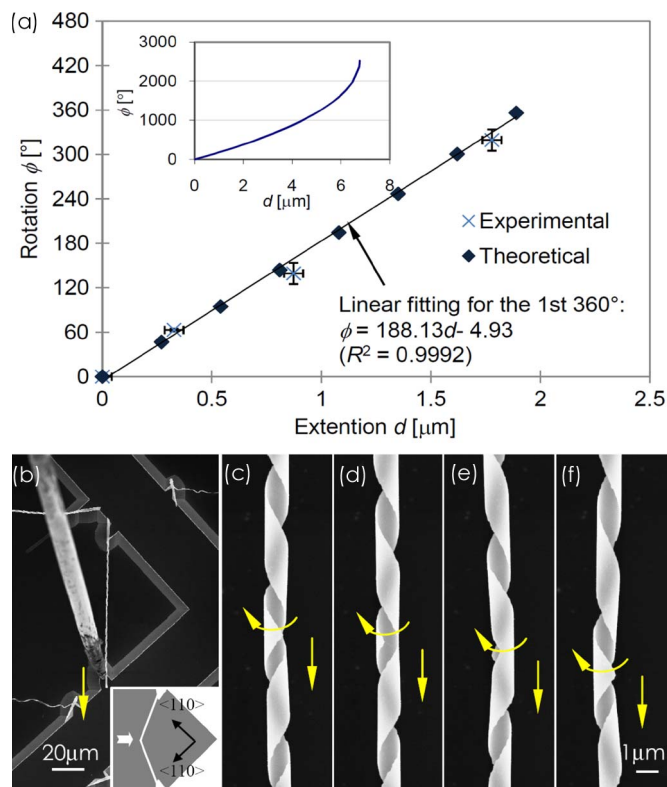


Fig. 2. Linear-to-rotary motion conversion ratio. (a) Linear-to-rotation (d to θ) conversion curve of a DCHNB ($\alpha_0 = 58^\circ$, $p_0 = 5.4 \mu\text{m}$, and $n = 7$) for the first turn (inset: Long range ϕ versus d curve). (b)–(f) *In situ* characterization of motion conversion using nanorobotic manipulation. (b) One end of an as-fabricated DCHNB (inset: A V-shaped mesa) is cut and attached to a “sticky” probe. (c)–(f) Rotation of the central part while moving the probe downward.

diameter of about $1 \mu\text{m}$. The helix is formed by an 8-nm-thick $\text{Si}_{0.6}\text{Ge}_{0.4}$ and a 10-nm-thick Si layer.

To implement and characterize motion converters, such as the one shown in Fig. 1(b), experimental investigations have been performed in a field emission scanning electron microscope (FESEM, Zeiss ULTRA 55) using a nanomanipulator (MM3A, Kleindiek) equipped with a tungsten probe [Picoprobe, T-4-10-1 mm, Fig. 2(b)] and an AFM cantilever (Mikromasch, CSC38/Ti-Pt, calibrated [32] stiffness: 0.1400 N/m). Manipulation of an as-fabricated DCHNB was performed by cutting the lower end of the DCHNB with the probe shown in Fig. 2(b). A “sticky” probe [33] is then prepared by dipping a Picoprobe into a silver tape and attached on the lower end of the DCHNB. Rotation is then generated in the central part [Fig. 2(c)–(f)] by moving the probe downward. We then measured the extension and rotation from Fig. 2(b)–(e) and plotted them in Fig. 2(a) [the DCHNB has the same parameters as that used in Fig. 2(a)]. It can be seen that the experimental and theoretical values are in excellent agreement.

IV. LOAD CONVERSION

In order to fully understand the load conversion, the mechanical properties of a DCHNB are characterized by cutting it and picking it up with a “sticky” probe as shown in Fig. 3(a)–(c). The free end of the DCHNB is then attached on an AFM cantilever and fixed with electron-beam-induced deposition

(EBID) [34], as shown in Fig. 3(d). Then, the tungsten probe attached to one end of a DCHNB is moved to the right to extend the DCHNB against an AFM cantilever using the nanomanipulator. Fig. 3(d)–(h) shows sequential SEM images showing the linear-to-rotary motion conversion. The generated rotary motion can be seen from the magnified frames. If both ends are equally displaced, the center of rotation will not translate in the axial direction. According to the apparent distance, the rotary angle ϕ can be determined. The ratio of linear-to-rotary motion conversion R_d is observed to be $171.3^\circ/\mu\text{m}$ according to Fig. 3(d)–(h). In the experiment, the radius of the tested DCHNB decreased approximately 4%, confirming that the radius change can be ignored. According to (3), the unwinding angle is calculated as $170.1^\circ/\mu\text{m}$ (2.47 turn/pitch), in good agreement with the experiment results.

Elongation versus tension curves [Fig. 3(i)] show that the stiffness in the first linear range is approximately 0.033 N/m . This is surprisingly small when compared to bottom-up synthesized carbon coils (0.12 N/m) [35] and ZnO nanosprings (4.2 N/m) [23] and comparable to the most compliant commercially available AFM cantilevers ($\sim 10^{-2} \text{ N/m}$). By using this device as a vision-based force sensor, the nanospring can provide a resolution of 11 pN/nm , assuming an imaging resolution of 1 nm . A low stiffness will facilitate the actuation of the motion converters. With large extension ($> 7 \mu\text{m}$), the stiffness becomes larger. The reasons for the nonlinearity of the stiffness are however not well understood yet. Several mechanisms are under investigation: 1) The HNBs have a prestressed two-layer structure (with one layer preextended and the other layer precompressed), so extension will make the internal stress redistributed; 2) the HNBs have stress competition between the longitudinal direction and the transverse direction [36], so extension stiffness is a resultant result due to this competition; and 3) the electron beam has a side effect on the nanobelts, including EBID [34] and hardening. These points may also be the reason why the stretching force did not return to zero at zero elongation for the second-round extension [Fig. 3(i)] besides SEM image drifting. It should be noted that, without the use of gears, bearings, or other types of pairs, such a “solid-state” motion converter will also be able to generate higher precision motion and will provide the possibility for measuring torque with a force sensor. This allows both higher precision positioning and more precise force application.

It is interesting to note that, due to the opposite chirality, the extension-induced torques at both ends can be self-compensated. This feature can be very useful for such applications as force measurement to avoid the side effect of end rotation as compressing or extending the other end.

Fig. 4(a)–(c) shows the characterization of the ratio of force-to-torque conversion using a probe and two AFM cantilevers (Mikromasch, CSC38/Ti-Pt, calibrated stiffness of cantilevers 1 and 2: 0.1400 and 0.0492 N/m). The ratio between the input force [Fig. 4(d)] and the output torque R_F [Fig. 4(e)] is found to be $2.110 \times 10^{-6} \text{ N} \cdot \text{m/N}$. This process resembles the application of the motion converter as a rotary stage for 3-D AFM. The investigation on the same nanospecimen from both axial and radial directions using two AFM cantilevers is the first demonstration of this type of device.

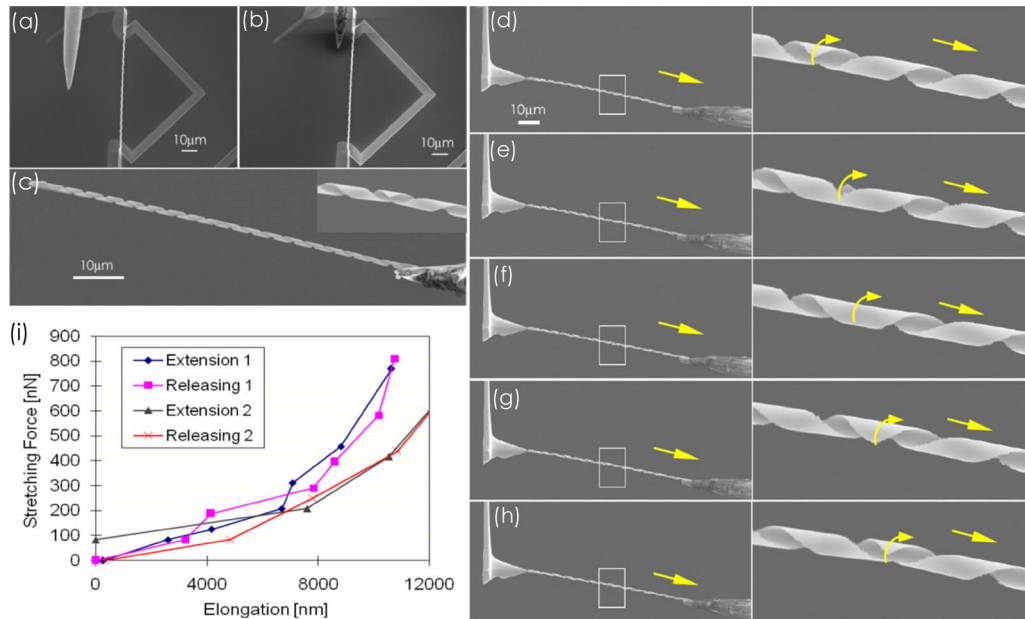


Fig. 3. Force-to-elongation characterization. (a)–(c) Manipulation of a DCHNB. (a) As-fabricated DCHNB with a tungsten probe for manipulation being visible. (b) Lower end of the DCHNB was broken with the probe shown in (a). A “sticky” probe is also visible. (c) DCHNB was picked up with a “sticky” probe. The inset shows the middle part. (d)–(i) Mechanical property characterization of a linear-to-rotary motion converter. (d)–(h) Sequential SEM images show the generation of rotary motion by pulling a tungsten probe attached to one end of a DCHNB against an AFM cantilever using a nanomanipulator in a FESEM. The ratio of linear-to-rotary motion conversion is $\sim 171.3^\circ/\mu\text{m}$. (i) Elongation versus tension curves show that the stiffness in the first linear range is ca. 0.033 N/m.

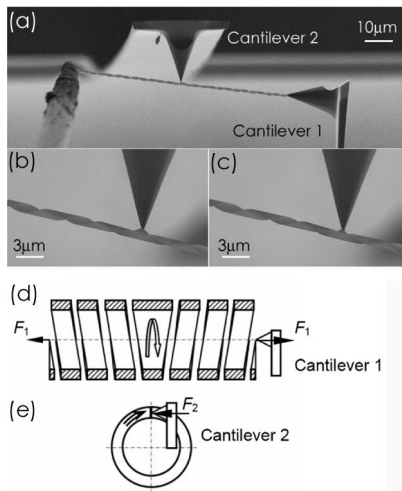


Fig. 4. Force-to-torque conversion ratio. (a)–(c) Ratio of force-to-torque conversion is characterized using a probe and two AFM cantilevers. The ratio between (d) the input force and (e) the output torque is found to be $2.110 \times 10^{-6} \text{ N} \cdot \text{m/N}$ (coil diameter: 947 nm; extension force F_1 : 1.280 nN; rotary force F_2 : 5.707 nN; torque: $2.702 \times 10^{-15} \text{ N} \cdot \text{m}$; rotary angle: 0.258 rad; torsional stiffness: $1.047 \times 10^{-14} \text{ N} \cdot \text{m/rad}$).

Extending the DCHNB more causes it to break [Fig. 5(a)]. The break occurred at the junction point of the two HNBS with opposite chirality [Fig. 5(b)]. It can also be seen from Fig. 5(b) that the shape of the HNBS remains unchanged as compared to the as-fabricated one. The broken section is along the cleavage direction $\langle 100 \rangle$, showing that it is possible to precisely break the DCHNB into two separate HNBS. Based on this, it is possible to clamp relatively large samples between the two HNBS, which can simplify the loading of the samples. By incorporating a gripper, sample loading can be further simplified.

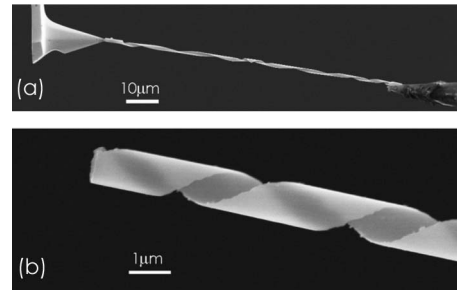


Fig. 5. Broken DCHNB. It can be seen that the break occurs at the middle point.

V. APPLICATION IN 3-D MICROSCOPY

A fundamental application of this type of motion converter is for 3-D microscopy. Fig. 6 shows 3-D imaging of a pollen grain. An Au-coated grain is first picked up by a Picoprobe (probe 1) and actuated with a manipulator [Fig. 6(a)]. Then, the probe is moved to a SiGe/Si/Cr DCHNB motion converter [Fig. 6(b)]. A DCHNB with narrow width and relatively big space between the adjacent turns has been selected for exposing the sample surface to the maximum. One end of the DCHNB has been cut and attached to a sticky Picoprobe (probe 2)—prepared by dipping a Picoprobe into a sticky silver tape. The pollen grain is then released from probe 1 by pushing the probe until the pollen attaches to the chip surface and then pushed toward the DCHNB to attach to it. Probe 2 is then moved downward to make the contact [Fig. 6(c)] and upward so that the motion converter with the attached pollen sample moves away from the substrate. A different imaging angle shows that the pollen only attached to the center of the DCHNB [Fig. 6(d)]. The motion converter has been characterized before loading the sample [Fig. 6(e)–(h)]. Fig. 6(i)–(l) shows that when

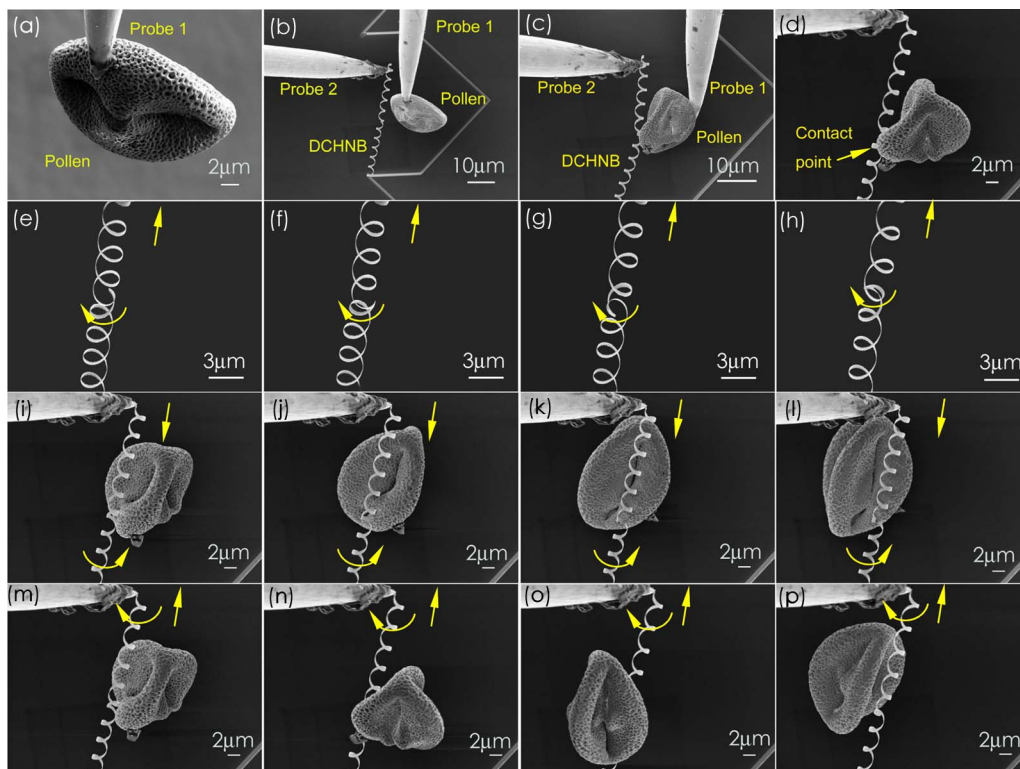


Fig. 6. Three-dimensional microscopy of a pollen grain. (a) Au-coated pollen grain is picked up by a Picoprobe (probe 1). (b) Probe is then moved to a DCHNB motion converter. One end of the DCHNB has been cut and attached to a sticky Picoprobe (probe 2). (c) Grain is then released from probe 1 by pushing the probe until the grain attaches to the chip surface, and then, the chip is pushed toward the DCHNB to attach. Probe 2 moves downward to make contact. (d) Probe 2 moves upward so that the motion converter with the attached pollen grain sample can detach from the substrate. A different imaging angle demonstrates that the pollen grain only attaches to the center of the DCHNB. (e)–(h) Motion converter has been characterized before loading the sample. (i)–(l) When releasing the extended DCHNB, the sample rotates counterclockwise (top view). (m)–(p) When stretching further the DCHNB, the sample rotates clockwise (top view).

releasing the extended DCHNB, the sample rotates counterclockwise (top view) for approximately 180° . Fig. 6(m)–(p) shows further stretching of the DCHNB, and the sample rotates clockwise (top view) for another 180° . Basically, for micro- and nanometer-scale samples, the deformation of the DCHNB due to the sample weight can be ignored. It can be seen that the different aspects of the sample can be exposed to the electron beam simply by extending or releasing the DCHNB with a small displacement. In the experiment, we have rotated the samples unidirectionally (clockwise from the top view) for four turns, leaving the DCHNB with no obvious residual changes in its shape. Further possibilities for this converter include goniometry for TEM, tomography for SEM or TEM, and 3-D SPM. Nanorobotic manipulation has been shown effective for sample attachment. For fixation, besides Van der Waals forces, EBID and FIB-induced deposition are optional approaches. By integrating in the fabrication processes of DCHNB, rolled-up spirals [37] can serve as claws for holding relatively large samples.

VI. CONCLUSION

In summary, a linear-to-rotary motion converter has been experimentally demonstrated with DCHNBs. The investigation has shown that the ratio of linear-to-rotary motion conversion is $171.3^\circ/\mu\text{m}$ length and the ratio of the output torque to the input force is $2.110 \times 10^{-6} \text{ N} \cdot \text{m/N}$. The stiffness (0.033 N/m)

is surprisingly small when compared to bottom-up synthesized helical nanostructures. In the torque measurement, two AFM cantilevers have been used for simultaneous characterization of axial and radial properties of the same nanostructure, which can be considered to be a prototype 3-D AFM. A fundamental application in 3-D imaging has been shown in a SEM using a pollen grain as a sample. Due to their extremely compact size, DCHNBs are well suited to serve as rotary scanners for creating 3-D SPMs, rotary stages for a microgoniometer for observing an object from different crystal surfaces, and components of nanomachines.

ACKNOWLEDGMENT

The authors would like to thank the FIRST Lab, ETH Zurich, for the support and D. Ziegler from the Nanotechnology Group, ETH Zurich, for calibrating the AFM cantilevers. The epitaxial growth of SiGe/Si was done at the Laboratory for Micro- and Nanotechnology, Paul Scherrer Institute.

REFERENCES

- [1] L. X. Dong and B. J. Nelson, "Robotics in the small—Part II: Nanorobotics," *IEEE Robot. Autom. Mag.*, vol. 14, no. 3, pp. 111–121, Sep. 2007.
- [2] Y. T. Yang, C. Callegari, X. L. Feng, K. L. Ekinci, and M. L. Roukes, "Zeptogram-scale nanomechanical mass sensing," *Nano Lett.*, vol. 6, no. 4, pp. 583–586, Apr. 2006.
- [3] M. Rief, F. Oesterhelt, B. Heymann, and H. E. Gaub, "Single molecule force spectroscopy on polysaccharides by atomic force microscopy," *Science*, vol. 275, no. 5304, pp. 1295–1297, Feb. 1997.

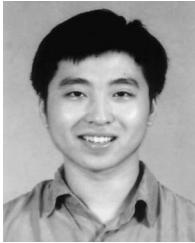
- [4] L. X. Dong, X. Y. Tao, L. Zhang, X. B. Zhang, and B. J. Nelson, "Nanorobotic spot welding: Controlled metal deposition with attogram precision from copper-filled carbon nanotubes," *Nano Lett.*, vol. 7, no. 1, pp. 58–63, Jan. 2007.
- [5] J. Cumings and A. Zettl, "Low-friction nanoscale linear bearing realized from multiwall carbon nanotubes," *Science*, vol. 289, no. 5479, pp. 602–604, Jul. 2000.
- [6] L. X. Dong, B. J. Nelson, T. Fukuda, and F. Arai, "Towards nanotube linear servomotors," *IEEE Trans. Autom. Sci. Eng.*, vol. 3, no. 3, pp. 228–235, Jul. 2006.
- [7] T. Ohki, S. V. Mikhailenko, M. F. Morales, H. Onishi, and N. Mochizuki, "Transmission of force and displacement within the myosin molecule," *Biochemistry*, vol. 43, no. 43, pp. 13 707–13 714, Nov. 2004.
- [8] G. Binnig, H. Rohrer, C. Gerber, and E. Weibel, "Surface studies by scanning tunneling microscopy," *Phys. Rev. Lett.*, vol. 49, no. 1, pp. 57–61, Jul. 1982.
- [9] G. Binnig, C. F. Quate, and C. Gerber, "Atomic force microscope," *Phys. Rev. Lett.*, vol. 56, no. 9, pp. 930–933, Mar. 1986.
- [10] E. W. Wong, P. E. Sheehan, and C. M. Lieber, "Nanobeam mechanics: Elasticity, strength, and toughness of nanorods and nanotubes," *Science*, vol. 277, no. 5334, pp. 1971–1975, Sep. 1997.
- [11] D. M. Eigler and E. K. Schweizer, "Positioning single atoms with a scanning tunneling microscope," *Nature*, vol. 344, no. 6266, pp. 524–526, Apr. 1990.
- [12] R. D. Piner, J. Zhu, F. Xu, S. H. Hong, and C. A. Mirkin, "Dip-pen nanolithography," *Science*, vol. 283, no. 5402, pp. 661–663, Jan. 1999.
- [13] H. J. Lee and W. Ho, "Single-bond formation and characterization with a scanning tunneling microscope," *Science*, vol. 286, no. 5445, pp. 1719–1722, Nov. 1999.
- [14] G. Binnig and H. Rohrer, "Scanning tunneling microscopy—From birth to adolescence," *Rev. Mod. Phys.*, vol. 59, no. 3, pp. 615–625, Jul. 1987.
- [15] C. Gerber and H. P. Lang, "How the doors to the nanoworld were opened," *Nat. Nanotechnol.*, vol. 1, no. 1, pp. 3–5, Oct. 2006.
- [16] R. Erlandsson, G. M. McClelland, C. M. Mate, and S. Chiang, "Atomic force microscopy using optical interferometry," *J. Vac. Sci. Technol. A, Vac. Surf. Films*, vol. 6, no. 2, pp. 266–270, Mar./Apr. 1988.
- [17] G. Meyer and N. M. Amer, "Novel optical approach to atomic force microscopy," *Appl. Phys. Lett.*, vol. 53, no. 12, pp. 1045–1047, Sep. 1988.
- [18] H. J. Dai, J. H. Hafner, A. G. Rinzier, D. T. Colbert, and R. E. Smalley, "Nanotubes as nanoprobe in scanning probe microscopy," *Nature*, vol. 384, no. 6605, pp. 147–150, Nov. 1996.
- [19] G. Binnig and D. P. E. Smith, "Single-tube 3-dimensional scanner for scanning tunneling microscopy," *Rev. Sci. Instrum.*, vol. 57, no. 8, pp. 1688–1689, Aug. 1986.
- [20] B. J. LeRoy, S. G. Lemay, J. Kong, and C. Dekker, "Scanning tunneling spectroscopy of suspended single-wall carbon nanotubes," *Appl. Phys. Lett.*, vol. 84, no. 21, pp. 4280–4282, May 2004.
- [21] B. J. LeRoy, I. Heller, V. K. Pahlwani, C. Dekker, and S. G. Lemay, "Simultaneous electrical transport and scanning tunneling spectroscopy of carbon nanotubes," *Nano Lett.*, vol. 7, no. 10, pp. 2937–2941, Oct. 2007.
- [22] S. Amelinckx, X. B. Zhang, D. Bernaerts, X. F. Zhang, V. Ivanov, and J. B. Nagy, "A formation mechanism for catalytically grown helix-shaped graphite nanotubes," *Science*, vol. 265, no. 5172, pp. 635–639, Jul. 1994.
- [23] X. Y. Kong and Z. L. Wang, "Spontaneous polarization-induced nanohelices, nanosprings, and nanorings of piezoelectric nanobelts," *Nano Lett.*, vol. 3, no. 12, pp. 1625–1631, Dec. 2003.
- [24] V. Y. Prinz, V. A. Seleznev, A. K. Gutakovskiy, A. V. Chehovskiy, V. V. Preobrazhenskii, M. A. Putyato, and T. A. Gavrilova, "Free-standing and overgrown InGaAs/GaAs nanotubes, nanohelices and their arrays," *Phys. E*, vol. 6, no. 1–4, pp. 828–831, Feb. 2000.
- [25] L. Zhang, E. Deckhardt, A. Weber, C. Schonenberger, and D. Grützmacher, "Controllable fabrication of SiGe/Si and SiGe/Si/Cr helical nanobelts," *Nanotechnology*, vol. 16, no. 6, pp. 655–663, Jun. 2005.
- [26] M. H. Huang, C. Boone, M. Roberts, D. E. Savage, M. G. Lagally, N. Shaji, H. Qin, R. Blick, J. A. Nairn, and F. Liu, "Nanomechanical architecture of strained bilayer thin films: From design principles to experimental fabrication," *Adv. Mater.*, vol. 17, no. 23, pp. 2860–2864, Dec. 2005.
- [27] D. J. Bell, L. X. Dong, B. J. Nelson, M. Golling, L. Zhang, and D. Grützmacher, "Fabrication and characterization of three-dimensional InGaAs/GaAs nanosprings," *Nano Lett.*, vol. 6, no. 4, pp. 725–729, Apr. 2006.
- [28] L. Zhang, E. Ruh, D. Grützmacher, L. X. Dong, D. J. Bell, B. J. Nelson, and C. Schonenberger, "Anomalous coiling of SiGe/Si and SiGe/Si/Cr helical nanobelts," *Nano Lett.*, vol. 6, no. 7, pp. 1311–1317, Jul. 2006.
- [29] P. X. Gao, W. J. Mai, and Z. L. Wang, "Superelasticity and nano-fracture mechanics of ZnO nanohelices," *Nano Lett.*, vol. 6, no. 11, pp. 2536–2543, Nov. 2006.
- [30] Y. G. Sun, W. M. Choi, H. Q. Jiang, Y. G. Y. Huang, and J. A. Rogers, "Controlled buckling of semiconductor nanoribbons for stretchable electronics," *Nat. Nanotechnol.*, vol. 1, no. 3, pp. 201–207, Dec. 2006.
- [31] A. W. Wahl, *Mechanical Springs*, 1st ed. Cleveland, OH: Penton, 1944.
- [32] J. E. Sader, J. W. M. Chon, and P. Mulvaney, "Calibration of rectangular atomic force microscope cantilevers," *Rev. Sci. Instrum.*, vol. 70, no. 10, pp. 3967–3969, Oct. 1999.
- [33] D. J. Bell, Y. Sun, L. Zhang, L. X. Dong, B. J. Nelson, and D. Grützmacher, "Three-dimensional nanosprings for electromechanical sensors," *Sens. Actuators A, Phys.*, vol. 130/131, pp. 54–61, Aug. 2006.
- [34] L. X. Dong, F. Arai, and T. Fukuda, "Electron-beam-induced deposition with carbon nanotube emitters," *Appl. Phys. Lett.*, vol. 81, no. 10, pp. 1919–1921, Sep. 2002.
- [35] X. Q. Chen, S. L. Zhang, D. A. Dikin, W. Q. Ding, R. S. Ruoff, L. J. Pan, and Y. Nakayama, "Mechanics of a carbon nanocoil," *Nano Lett.*, vol. 3, no. 9, pp. 1299–1304, Sep. 2003.
- [36] L. Zhang, D. D. Xu, L. X. Dong, and B. J. Nelson, "Aging effect of rolled-up InGaAs/GaAs/Cr helical nanobelts," *Microelectron. Eng.*, vol. 86, no. 4–6, pp. 824–827, Apr.–Jun. 2009.
- [37] L. Zhang, L. X. Dong, D. J. Bell, B. J. Nelson, C. Schönenberger, and D. Grützmacher, "Fabrication and characterization of freestanding Si/Cr micro- and nanospirals," *Microelectron. Eng.*, vol. 83, no. 4–9, pp. 1237–1240, Apr.–Sep. 2006.



Lixin Dong (S'01–M'03) received the B.S. and M.S. degrees in mechanical engineering from Xi'an University of Technology (XUT), Xi'an, China, in 1989 and 1992, respectively, and the Ph.D. degree in microsystems engineering from Nagoya University, Nagoya, Japan, in 2003.

He became a Research Associate in 1992, a Lecturer in 1995, and an Associate Professor in 1998 at XUT. In 2003, he became an Assistant Professor at Nagoya University. In 2004, he joined the Swiss Federal Institute of Technology (ETH) Zurich, Zurich, Switzerland, as a Research Scientist, where he became a Senior Research Scientist in 2005 and led the NanoRobotics Group, Institute of Robotics and Intelligent Systems. Since December 2008, he has been an Assistant Professor at Michigan State University, East Lansing. His current research interests include nanorobotics, nanoelectromechanical systems, mechatronics, mechanochemistry, and nanobiomedical devices.

Dr. Dong is an Associate Editor of the IEEE TRANSACTIONS ON NANOTECHNOLOGY and the IEEE TRANSACTIONS ON AUTOMATION SCIENCE AND ENGINEERING. He received the IEEE TRANSACTIONS ON AUTOMATION SCIENCE AND ENGINEERING (T-ASE) Googol Best New Application Paper Award in 2007 and the Best Conference Paper Award at the International Conference on Computer Science and Education 2003. He was a finalist for the Best Paper Awards at the IEEE International Conference on Robotics and Automation (ICRA) 2007, the IEEE/RSJ International Conference on Intelligent Robots and Systems 2005, and ICRA 2001. He has been awarded the Science and Technology Advancement Prize by the Ministry of Education of China in 1999, by the Shaanxi Province Government in 1995 and 1999, by the Xi'an City Government in 1999, and by the Ministry of Machine-Building Industry of China in 1998 and 1992.



Li Zhang received the B.S. degree from the Department of Materials Science and Engineering, Zhejiang University, Hangzhou, China, in 2000, the M.S. degree from the Department of Materials Science and Engineering, Christian Albrechts University, Kiel, Germany, in 2002, and the Ph.D. degree from the University of Basel, Basel, Switzerland, in 2007.

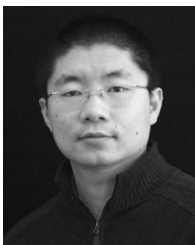
From 2002 to 2006, he was with the Laboratory for Micro- and Nanotechnology, Paul Scherrer Institute, and also with the Department of Physics, University of Basel. In 2007, he joined the Institute of Robotics and Intelligent Systems, Swiss Federal Institute of Technology (ETH) Zurich, Zurich, Switzerland, as a Postdoctoral Researcher, where he is currently a Senior Research Scientist. His current research interests include micro/nanofabrication, wireless sensing and actuation, and micro/nanoelectromechanical systems devices.

Dr. Zhang received the Chinese Government Award for Outstanding Self-financed Students Abroad in 2005 from the China Scholarship Council and the Best Automation Paper Award—Finalist at the 2007 IEEE International Conference on Robotics and Automation.



Bradley E. Kratochvil (S'04) received the B.S. degree in computer engineering from the University of Nebraska, Lincoln, in 2001, the M.S. degree in computer science from the University of Minnesota, Minneapolis, in 2003, and the Ph.D. degree from the Swiss Federal Institute of Technology (ETH) Zurich, Zurich, Switzerland, in 2008. His doctoral work concentrated primarily on visual tracking and 3-D reconstruction of nanorobotic manipulations in a scanning electron microscope.

He is currently a Postdoctoral Associate with the Institute of Robotics and Intelligent Systems, ETH Zurich, focusing his research on micro/nanomanipulation, computer vision for microscopy, and untethered mobile microrobots.



Kaiyu Shou received the B.S. degree from the Department of Automation and Control Engineering, Xi'an Jiaotong University (XJTU), Xi'an, China, in 1999, and the M.E. degree in the Institute of Systems Engineering, XJTU, in 2003. Since April 2006, he has been working toward the Ph.D. degree in the Institute of Robotics and Intelligent Systems, Swiss Federal Institute of Technology (ETH) Zurich, Zurich, Switzerland.

In 2000, he joined the Institute of Systems Engineering. During that period, he worked on dynamics analysis and controller design of a 6-DOF parallel robot. In 2003, he was a Research Assistant at the Robotics Research Institute, University of Dortmund, Dortmund, Germany. His research focused on robot force control at that time. His current research interests include design, simulation, drive, and control of nanoelectromechanical systems.



Bradley J. Nelson (M'90–SM'06) received the B.S. degree in mechanical engineering from the University of Illinois, Urbana, in 1984, the M.S. degree in mechanical engineering from the University of Minnesota, Minneapolis, in 1987, and the Ph.D. degree in robotics from the School of Computer Science, Carnegie Mellon University, Pittsburgh, PA, in 1995.

He was an Engineer with Honeywell and Motorola and served as a U.S. Peace Corps Volunteer in Botswana, Africa. He became an Assistant Professor at the University of Illinois, Chicago, in 1995, and an Associate Professor at the University of Minnesota in 1998. Since 2002, he has been a Professor in the Institute of Robotics and Intelligent Systems, Swiss Federal Institute of Technology (ETH) Zurich, Zürich, Switzerland. His current research interest includes extending robotics research into emerging areas of science and engineering. His most recent scientific contributions have been in the area of microrobotics, biomicrobotics, and nanorobotics, including efforts in robotic micromanipulation, microassembly, microelectromechanical systems (sensors and actuators), mechanical manipulation of biological cells and tissue, and nanoelectromechanical systems. He has also contributed to the fields of visual servoing, force control, sensor integration, and Web-based control and programming of robots.

Dr. Nelson has been a member of the Editorial Boards of the IEEE TRANSACTIONS ON ROBOTICS, the IEEE TRANSACTIONS ON NANOTECHNOLOGY, the *Journal of Micromechatronics*, the *Journal of Optomechatronics*, and the *IEEE Robotics and Automation Magazine*. He was elected as a Robotics and Automation Society Distinguished Lecturer in 2003 and won Best Paper Awards at major robotics conferences and journals in 2004, 2005, 2006, 2007, 2008, and 2009. He was named to the 2005 "Scientific American 50," *Scientific American* magazine's annual list recognizing 50 outstanding acts of leadership in science and technology from the past year for his efforts in nanotube manufacturing. His laboratory won the 2007 and 2009 RoboCup Nanogram Competition, both times the event has been held. He has chaired several international workshops and conferences, has served as the Head of the Department of Mechanical and Process Engineering from 2005 to 2007, and is currently the Chairman of the Board of Directors of the ETH Electron Microscopy Center (EMEZ). He has been awarded a McKnight Land-Grant Professorship. He is a recipient of the Office of Naval Research Young Investigator Award, the National Science Foundation Faculty Early Career Development (CAREER) Award, the McKnight Presidential Fellows Award, and the Bronze Tablet.